The Astrophysical Journal, 638:987–1003, 2006 February 20

EARLY INFRARED SPECTRAL DEVELOPMENT OF V1187 SCORPII (NOVA SCORPII 2004 NO. 2)

D. K. Lynch,[1,2] C. E. Woodward,[3] T. R. Geballe,[4] R. W. Russell,[1,2] R. J. Rudy,[1] C. C. Venturini,[1]
G. J. Schwarz,[5] R. D. Gehrz,[2,3] N. Smith,[2,6] J. E. Lyke,[7] S. J. Bus,[8] M. L. Sitko,[2,9]
T. E. Harrison,[10] S. Fisher,[4] S. P. Eyres,[11] A. Evans,[12] S. N. Shore,[13] S. Starrfield,[14]
M. F. Bode,[15] M. A. Greenhouse,[16] P. H. Hauschildt,[17] J. W. Truran,[18]
R. E. Williams,[19] R. Brad Perry,[2,20] R. Zamanov,[15] and T. J. O'Brien[21]

Received 2005 June 2; accepted 2005 September 19

ABSTRACT

We report on an unprecedented infrared time series of spectra of V1187 Sco, a very fast ONeMg nova. The observations covered a 56 day period (2004 August 6–September 30) starting 2 days after the nova's peak brightness. Time evolution of the spectra revealed changing line strengths and profiles on timescales of less than a day to weeks as the nova evolved from early postmaximum to early coronal phases. When our ground-based optical and *Spitzer Space Telescope* data were combined, the wavelength coverage of 0.38–36 μm allowed an accurate spectral energy distribution to be derived when it was about 6 weeks after outburst. Developing double structure in the He I lines showed them changing from narrow to broad in only a few days. Using the O I lines in combination with the optical spectra, we derived a reddening of $E(B-V) = 1.56 \pm 0.08$ and a distance of 4.9 ± 0.5 kpc. Modeling of the ejected material strongly suggested that it was geometrically thick with $\Delta R/R = 0.8$–0.9 (more of a wind than a shell) and a low filling factor of order a few percent. The line shapes were consistent with a cylindrical jet, bipolar, or spherical Hubble flow expansion with a maximum speed of about -3000 km s^{-1}. The central peak appeared to be more associated with the spherical component, while the two peaks (especially in Hβ) suggested a ring with either a lower velocity component or with its axis inclined to the line of sight.

Subject headings: infrared: stars — novae, cataclysmic variables — stars: individual (V1187 Scorpii)

1. INTRODUCTION

Novae are of astrophysical interest for many reasons. Along with supernovae and red giants, they enrich the interstellar medium with heavy elements (Gehrz et al. 1998). The material expelled in the thermonuclear runaway (TNR) is a mixture of partially burned hydrogen accreted from the secondary star and material entrained from the surface of the white dwarf (WD). Variations in the WD mass, luminosity, composition, and accretion rate produce ejecta that display a wide variety of properties. Outbursts on ONeMg WDs produce enhancements (relative to solar) in some elements such as C, N, O, Mg, Ne, Al, and sometimes S (Vanlandingham et al. 2005; Schwarz 2002; Shore et al. 2003).

The dynamics and physics of TNRs is also of interest because the burning surface material is not confined to the stellar interior but rather is more or less free to expand and cool, thereby quenching the nuclear reactions before they reach equilibrium. In very fast novae such as V1187 Sco, the proton capture rates exceed the β-decay rates, thereby changing the elemental composition of the ejecta in a way that can be diagnostic of the evolution of the TNR. Furthermore, the spatial structure of the ejecta is probably determined very close to the WD and therefore fairly early in the event. This is revealed later by blobs and density inhomogeneities that can be modeled to ultimately understand the hydrodynamics and turbulence in the dynamical evolution of the runaway and the ejecta.

Our knowledge of the evolution of novae is always hampered by a lack of time-resolved spectra. Without detailed knowledge of how the spectra change with time, it is impossible to model the shell, i.e., is it optically thin, blobby, or subject to dynamical variations between observations? The appearance and disappearance

[1] The Aerospace Corporation, Mail Stop 2-266, P.O. Box 92957, Los Angeles, CA 90009-2957; david.k.lynch@aero.org.
[2] Visiting Astronomer at the Infrared Telescope Facility, which is operated by the University of Hawaii under Cooperative Agreement NCC 5-538 with the NASA, Office of Space Science, Planetary Astronomy Program.
[3] Department of Astronomy, University of Minnesota, 116 Church Street, SE, Minneapolis, MN 55455.
[4] Gemini Observatory, 670 North A'ohoku Place, Hilo, HI 96720.
[5] Steward Observatory, University of Arizona, 933 North Cherry Avenue, Tucson, AZ 85721.
[6] Center for Astrophysics and Space Astronomy, University of Colorado, 389 UCB, Boulder, CO 80309.
[7] W. M. Keck Observatory, 65-1120 Mamalahoa Highway, Kamuela, HI 96743.
[8] Institute for Astronomy, University of Hawaii, 640 North A'ohoku Place, Hilo, HI 96720.
[9] Department of Physics, University of Cincinnati, 400 Geology/Physics Building, P.O. Box 210011, Cincinnati, OH 45221-0011.
[10] Department of Astronomy, New Mexico State University, Department 4500, Box 30001, Las Cruces, NM 88003.
[11] Department of Physics, Astronomy and Mathematics, University of Central Lancashire, Preston PR1 2HE, UK.
[12] Department of Physics, Keele University, Keele, Staffordshire ST5 5BG, UK.
[13] Dipartimento di Fisica "Enrico Fermi," Università di Pisa, and INFN, Sezione di Pisa, Largo B. Pontecorvo 3, I-56127 Pisa, Italy.
[14] Department of Physics and Astronomy, Arizona State University, Box 871504, Tempe, AZ 85287-1504.
[15] Astrophysics Research Institute, Liverpool John Moores University, Twelve Quays House, Birkenhead CH41 1LD, UK.
[16] NASA Goddard Space Flight Center, Code 665, Greenbelt, MD 20771.
[17] Hamburger Sternwarte, Gojenbergsweg 112, 21029 Hamburg, Germany.
[18] Department of Astronomy and Astrophysics, University of Chicago, 5640 South Ellis Avenue, Chicago, IL 60637; and Argonne National Laboratory.
[19] Space Telescope Science Institute, 3700 San Martin Drive, Baltimore, MD 21218.
[20] NASA Langley Research Center, A1/Science Support Office, Hampton, VA 23681.
[21] Jodrell Bank Observatory, University of Manchester, Macclesfield, Cheshire SK11 9DL, UK.

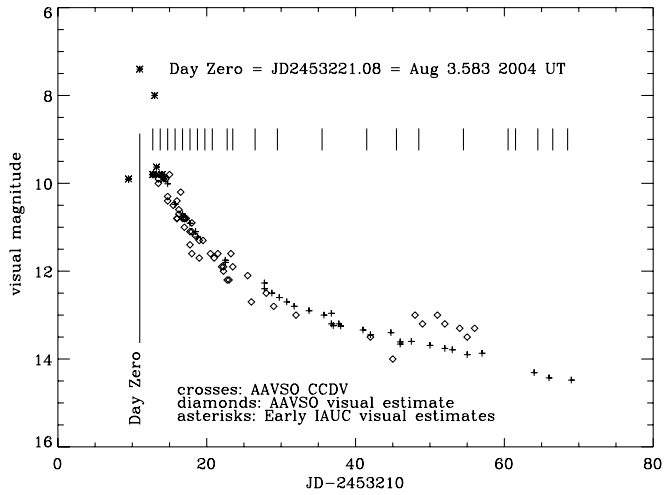

FIG. 1.—Light curve from the AAVSO and IAU Circulars. The dates of our observations from Table 1 are indicated by the vertical lines above the light curve. V1187 Sco's light curve shows a fast, monotonic decline with no evidence of extinction by dust formation. Owing to uncertainties in the brightest points and the actual time of peak brightness, the derived decline rates can vary. We find 2 days $< t_2 <$ 8.7 days and 5 days $< t_3 <$ 15 days, making this nova one of the fastest ever observed.

of lines with time and their relation to different species provides important information about the excitation and ionization conditions in the shell. Most well-studied novae have been done in the optical, but the optical lines only reveal information (primarily) about the electronic transitions. Observations in the infrared have the advantage of low extinction, the presence of molecular and coronal lines, and information about the formation and composition of dust. The fortunate circumstances of having a number of nova observers on large telescopes during the outburst of V1187 Sco has provided an unprecedented opportunity to study the early stages of ejecta development over a wide range of wavelengths.

V1187 Sco was discovered prior to peak brightness based on an unfiltered CCD image by A. Takao on 2003 August 3.583 UT when it was around $m_V = 7.4$ (Yamaoka 2004). All Sky Automated Survey (ASAS)-3 patrol images for the previous day (August 2.071) showed the object at $m_V = 9.9$. On August 5.49, Yamaoka reported that a low-resolution spectrum taken by M. Fujii showed 3000 km s^{-1} wide (FWHM) Hα and Hβ emission lines with P Cygni profiles (Yamaoka et al. 2004), all consistent with a classical nova in its early postmaximum phase.

Figure 1 shows the American Association of Variable Star Observers (AAVSO) light curve. Based on these data, we adopted the discovery date (2004 August 3.583, JD 2,453,221.08) as the date of peak brightness. The rate of decline was prodigious: $t_2 = 2$ and $t_3 = 5$ days; however, the first two data points at maximum are suspect because they were obtained from unfiltered CCD images and under poor sky conditions, respectively. The decline determined from the remaining data was still large, with $t_2 = 8.7$ and $t_3 = 15$ days, and indicates that V1187 Sco is a "very fast" nova (Payne-Gaposchkin 1957). We have adopted the latter values for t_2 and t_3 in the distance and reddening analyses. Theoretical light curves (Kato 2002) suggest that light curves of this speed and shape correspond to TNRs on massive WDs, certainly with $M_{\rm WD} \geqslant 1.2\ M_\odot$.

In this paper we report visible and infrared spectroscopy from a variety of instruments over a 56 day period (2004 August 5–September 30) starting 2 days after the nova's peak brightness. Twenty-three spectra were obtained. Of particular note are the *Spitzer Space Telescope*'s first published nova outburst spectrum (5–28 μm) and nearly simultaneous MMT (0.38–0.87 μm) and Infrared Telescope Facility (IRTF)/Keck/United Kingdom Infrared Telescope (UKIRT) (0.8–2.5 μm) spectra, leading to a spectral energy distribution determination that uses data covering a factor of 82 in wavelength.

2. OBSERVATIONS

The spectroscopy reported here came from six telescopes and seven instruments: the IRTF with Broadband Array Spectrograph System (BASS; Hackwell et al. 1990) and SpeX (Rayner et al. 2003), Gemini's Gillett Telescope (North) with MICHELLE (Glasse et al. 1997), UKIRT with Cooled Grating Spectrometer 4 (CGS4; Mountain et al. 1990), Keck with NIRSPEC (McLean et al. 1998), the MMT with the optical spectrograph, and *Spitzer* with Infrared Spectrograph (IRS; Houck et al. 2004). Table 1 shows the observation log.

The BASS spectra were obtained using a 3.″3 diameter circular aperture with an 18″ north-south chop and nod in the standard double beam mode. The flux model for the calibration star α Boo was consistent with that of Cohen et al. (1992a, 1992b, 1995, 1996, 1998) to within a few percent at every wavelength. Both objects were near the same air mass ($\sim$1.9), and no extinction corrections were made.

Mid-infrared spectra of V1187 Sco were obtained at the Frederick C. Gillett Gemini Telescope (Gemini North) on Mauna Kea on the nights of UT 2004 August 11 and September 7 and 26 in photometric conditions, using the facility 7–25 μm imaging spectrograph Michelle (Glasse et al. 1997). On each night the instrument was configured with its "lowN" grating and 0.″4 wide slit to cover the 7–13 μm region at a resolving power of 200. Standard chopping and nodding procedures were used. On each night spectra of either BS 6879 (B9.5 III; $T = 10,000$ K and $N = 1.6$ assumed) and BS 6165 (B0 V; $T = 20,000$ K and $N = 3.8$ assumed) were observed before or after the nova and used to provide wavelength calibration accurate to better than 0.01 μm (3 σ), remove telluric absorption features, and allow flux calibration accurate to $\pm$30%.

Spectra in the 1–5 μm region were obtained at UKIRT on Mauna Kea, using its facility spectrographs UKIRT Imager Spectrometer (UIST) and CGS4 (Mountain et al. 1990), on the nights of UT 2004 September 3 and 4. UIST was used to cover 1.4–5.2 μm, and CGS4 covered 0.8–1.35 μm. UIST was configured with a 0.″24 wide slit and various grisms to cover the four observed wave bands. CGS4 was configured with a 0.″6 wide slit and its 40 line mm^{-1} grating. All UKIRT observations were taken in stare mode and included frequent nodding along the slit. Wavelength calibration was derived from spectra of either arc lamps or comparison stars and is accurate to better than 0.0005 μm (3 σ) in all UKIRT wave bands. Fluxes of comparison stars at infrared wavelengths were estimated from their visual magnitudes and the infrared colors for stars of their spectral types given in Tokunaga (2000). Prominent hydrogen recombination lines were removed from the spectra of the comparison stars prior to ratioing.

The IRTF SpeX data were obtained on 2004 September 28 UT using a $0.''8 \times 15''$ slit and a 10″ north-south nod for background cancellation. No chopping was performed, and extinction corrections were not necessary because of the proximity of the calibrators. Data reduction was done using SpeXTools (Cushing et al. 2004). For most of the observations HD 161822 and HD 157486 were used as calibrators, but for the longer wavelength measurements on September 16 we used HD 162220. Flux models were obtained by taking the V magnitude and spectral type

TABLE 1
Observing Log

Date (UT)	Age (days)	JD (Nearest)	Telescope	Instrument	Wavelength (μm)
Aug 5.35	2	2453225.5	IRTF	BASS	3–14
Aug 6.24	3	2453226.5	IRTF	BASS	3–14
Aug 7.19	4	2453227.5	IRTF	BASS	3–14
Aug 7.18	4	2453227.5	KPNO 4 m	RCSP	0.37–0.51
Aug 8.19	5	2453228.5	IRTF	BASS	3–14
Aug 9.19	6	2453229.5	IRTF	BASS	3–14
Aug 10.19	7	2453230.5	IRTF	BASS	3–14
Aug 11.19	8	2453231.5	IRTF	BASS	3–14
Aug 11.25	8	2453231.5	Gemini North	Michelle	7–13
Aug 12.19	9	2453232.5	IRTF	BASS	3–14
Aug 13.2	10	2453233.5	IRTF	SpeX	0.85–2.5
Aug 15.19	12	2453235.5	IRTF	BASS	3–14
Aug 15	12	2453235.5	IRTF	SpeX	0.85–2.5
Aug 19	16	2453239.5	IRTF	SpeX	0.85–2.5
Aug 22.3	19	2453242.5	Keck	NIRSPEC	0.95–1.14
Aug 23.3	20	2453243.5	Keck	NIRSPEC	1.15–2.55
Aug 28	25	2453248.5	IRTF	SpeX	0.85–2.5
Sep 3	31	2453254.5	UKIRT	CGS4	0.8–1.35
Sep 3	31	2453254.5	UKIRT	UIST	1.4–5.2
Sep 4	32	2453255.5	UKIRT	CGS4	0.8–1.35
Sep 4	32	2453255.5	UKIRT	UIST	1.4–5.2
Sep 7	35	2453258.5	Gemini North	Michelle	7–13
Sep 10	38	2453261.5	IRTF	SpeX	0.85–2.5
Sep 16	44	2453267.5	IRTF	SpeX	2.4–5.5
Sep 22	50	2453273.5	IRTF	SpeX	0.85–2.5
Sep 23.1	51	2453274.5	MMT	Spectrograph	0.38–0.87
Sep 26	54	2453277.5	Gemini North	Michelle	7–13
Sep 28.4	56	2453279.5	*Spitzer*	IRS	5–38
Sep 30	58	2453281.5	IRTF	SpeX	0.85–2.5

from the Bright Star Catalog (Hoffleit & Jaschek 1982)[22] and assuming that their shapes matched the models from Kurucz (1991, 1994). Small adjustments were made to the width and strength of the stronger stellar absorption features (e.g., the calcium infrared triplet and the Paschen lines) in the models to match the actual observations. An absolute flux scale was determined by normalizing to the K magnitude that was calculated from the V magnitudes and the $V-K$ color for stars of the calibrators' spectral types tabulated by Koornneef (1983).

Near-infrared spectra of V1187 Sco were obtained on 2004 August 22.27 and 23.25 UT on the Keck II telescope using NIRSPEC (McLean et al. 1998) in low-resolution mode with a $0\farcs38 \times 42''$ slit. Multiple spectra, within the bandpass of the order-sorting filters, were obtained by nodding the source along the slit at $15''$ intervals while guiding on the slit. The telluric standards HD 162220 and HD 163633 were observed in a similar manner. The two-dimensional spectral images of both the nova and the telluric standards were processed using standard infrared techniques (Joyce 1992) using the REDSPEC reduction software. Flux calibration of the nova spectra from 0.94 to 1.14 μm and from 1.15 to 2.55 μm was performed by using the spectrum of HD 162220 and HD 163633, respectively, normalized by a blackbody source function with $T_{\rm eff} = 9480$ K (Tokunaga 2000), appropriate to their spectral type (A0 V) and Two Micron All Sky Survey (2MASS) magnitudes (HD 162220: $J = 6.481$, $H = 6.472$, $K_s = 6.450$; HD 163633: $J = 9.192$, $H = 9.054$, $K_s = 9.035$). Residual absorption from hydrogen lines in the stellar spectra were removed by linear interpolation of the continuum adjacent to the feature prior to division of the object spectrum. However, the intrinsic hydrogen lines near 1.875 and 1.944 μm were not removed, as these lines occurred in noisy parts of the calibrator spectrum and their removal introduced serious fringing in the final spectra. On NIRSPEC, the K band is divided between two settings of the cross disperser, and the 2MASS K_s filter center falls along the overlap of the two settings. Despite wavelength overlap, there was a flux difference noted between the two settings. The flux density of the K-long part of the spectrum is about 10% below the K_s part of the spectrum. We have applied a renormalization correction to the K-long flux to account for this discrepancy. As the seeing on both nights was $0\farcs7$–$0\farcs9$, we estimate that the absolute photometry is accurate to approximately 10% due to slit loss.

Optical spectra were obtained at the MMT on the night of 2004 September 23.09 UT using the Blue Channel spectrograph (Schmidt et al. 1989) in long-slit mode ($1'' \times 180''$ slit) with the 300 line mm^{-1} grating and a single grating setting centered at 6000 Å under $0\farcs6$ seeing. The spectral resolution was approximately 900 with a dispersion of 1.95 Å pixel^{-1} resulting in a wavelength coverage from 3400 to 8670 Å. All data reduction and extractions were performed using the IRAF package SPECRED. The nova and spectroscopic standard frames were bias subtracted, flat fielded using quartz lamp exposures, individually extracted, and wavelength calibrated using exposures of a HeAr arc lamp. The individual nova spectra were then flux calibrated using the spectroscopic standards Feige 110 and BD +28 4211 (the flux templates for these sources are provided in the IRAF routines) and then co-added to produce the final spectrum.

[22] Also Vizier Online Data Catalog, 50 (Hoffleit & Warren, 1995).

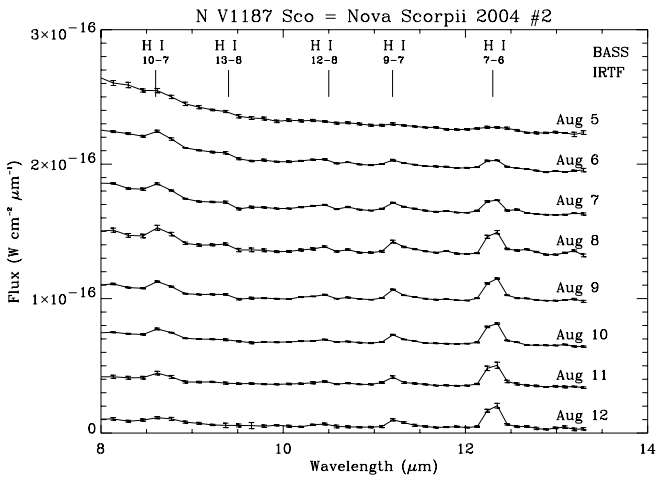

FIG. 2.—The 8–13 μm time sequence of BASS data. The earliest spectrum is on top, and the latest is on the bottom. The bottom spectrum has the correct flux calibration. All the rest have been shifted successively upward by 3×10^{-17} W cm^{-2} μm^{-1} to enhance visibility. The strongest line is Huα, which is barely discernible against the continuum in the first night but rapidly grows on each successive night, as do the other H I lines.

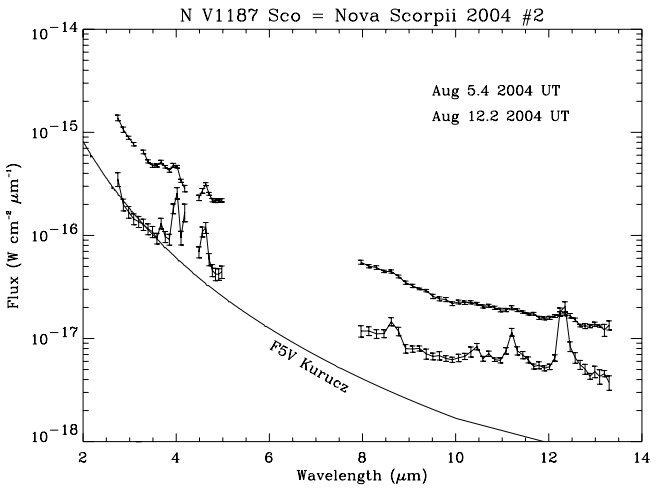

FIG. 3.—First and last BASS/IRTF spectra on the same scale and a scaled spectrum of an F5 V star shown for comparison. The continuum is clearly non-Planckian, with excess emission longward of 9 μm both early and late.

V1187 Sco was observed by the *Spitzer* on 2004 September 28.40 UT using IRS (Werner et al. 2004; Houck et al. 2004) as part of the Cycle 1 nova target of opportunity proposal PID 2316 (AOR key 10274816). The IRS peak-up array was not used; instead placement of the nova in the spectrograph slit relied on the excellent inertial pointing of the spacecraft (1″ rms) and astrometric coordinates obtained from IAU Circulars. The low-resolution IRS data were reduced using the following general methodology after retrieving data from the pipeline processed (ver. 11) archive. Individual data collection events obtained at two different slit positions (target nodded along the slit) were differenced in IRAF to subtract residual background. This was performed on the two-dimensional basic calibration data products. SPICE (beta ver. 8.0) extraction was then performed on each background-subtracted two-dimensional image. Default extraction widths were used (4 pixels wide at 6 μm and 8 pixels wide at 12 μm) to ensure accurate point-source fluxing. The individual extracted spectra (four each for a given order in channel 0) were then combined using a weighted linear combination to produce a single output spectrum. The standard deviation at a given wavelength represents the statistical variance of the flux at that pixel. In wavelength regions where IRS spectral orders overlapped, the data were combined using a simple average, and the uncertainty in the flux was determined by a quadrature sum of the errors. No attempt was made to normalize the continuum flux between the two spectral segments measured from different orders. We note that data shortward of approximately 8 μm and longward of approximately 14.5 μm in the first-order spectra are not considered "valid" due to order overlap issues, and we ignore these data. The spectral lines were then fitted using a least-squares Gaussian routine that fitted the line amplitude, continuum level, slope of continuum, and line center. The FWHM was determined from examining individual isolated H recombination lines in a full Gaussian fit, then this FWHM was held constant for all other lines (FWHM = 0.1185 μm in this data set). Lines that appeared exceptionally broad were fitted with double Gaussians of equal fixed width (FWHM = 0.1185 μm) to estimate the position and required fluxes of multiple lines that potentially contribute to the observed emission. Line identifications were determined by wavelength association of emission features, comparison of the spectra of V1187 Sco (which has forbidden lines) with *Spitzer* spectra of V1186 Sco (dominated by H recombination lines), and comparison of the V1187 Sco Gemini Michelle spectra (similar resolution) to that of the *Spitzer* data.

The astronomical observing template employed for the IRS high-resolution observations (channel 3) was obtained in STARE mode. Thus, background subtraction of these data was not attempted because the point-spread function of the nova filled a significant fraction of the slit area. Individual "hot" pixels in the extracted spectra were clipped and replaced with values derived from linear interpolation of adjacent pixels. Beside broad emission lines evident in the IRS high-resolution data (e.g., [O IV] at 25.91 μm), narrow emission features (of order 3 pixels) are present that are likely due to line-of-sight interstellar cirrus emission.

Owing to the variety of instruments, telescope apertures, calibrator stars, and flux models, we cannot claim absolute photometric accuracy to better than about 20%–30%. Judging from the repeatability of weak features from different instruments, however, we believe that the relative photometric accuracy is probably better than a few percent within each spectrum.

3. THERMAL INFRARED AND CONTINUUM (DAYS 2–9)

Our first observations were on the IRTF with BASS on the night of 2004 August 5.4, about 2 days after peak brightness. To our knowledge this is the earliest that a nova has ever been observed spectroscopically in the 10 μm region. Figure 2 shows the 8–13 μm time series of BASS spectra covering the time interval August 5–12 (days 2–9). Initially the nova showed a smooth, continuum with only a hint of emission from H I (7–6) Huα and H I (10–7). The next night H I emission lines from the Humphreys, Pfund, and higher levels appeared and doubled in strength during each of the next few nights. They then grew more slowly over most of the remainder of the observing period.

The shape of the earliest spectrum (2004 August 5.4 UT) and a later spectrum (2004 August 12.2 UT) are shown in Figure 3 along with a scaled 1500 K blackbody curve. The emission was presumably the infrared equivalent of the F-type spectrum commonly seen in the visible in novae near maximum (Warner 1989).

4. THERMAL INFRARED LINE EMISSION (DAYS 8, 35, AND 54)

The Gemini spectra spanned the time interval August 11–September 26. H I lines from the $n = 6$, 7, 8, and 9 series are clearly evident in the earliest spectrum, and most of them can be

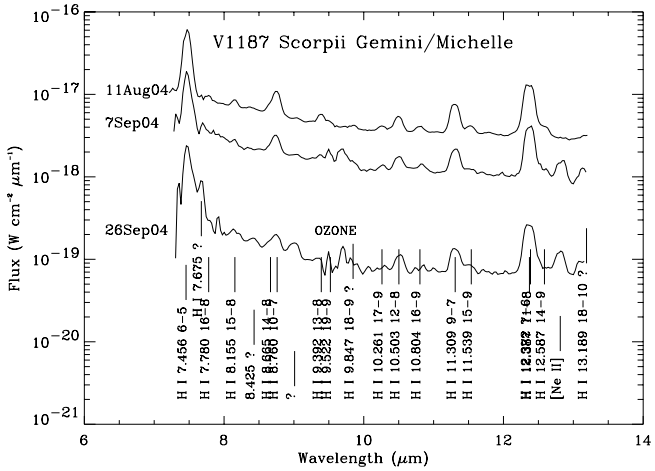

FIG. 4.—Gemini Spectra obtained on August 11 and September 7 and 28. No scaling or shifting of the spectra was done. The overall fading of the object is evident, as is the emergence of the [Ne II] line at 12.8 μm. Two lines remain unidentified: 8.425 and 9.01 μm.

seen in the subsequent spectra (Fig. 4). A complete listing is provided in Table 2. Note that some of the H I lines are blended with others. To our knowledge lines from the n–9 series have never before been seen in an astronomical object. The stronger H I lines show roughly Gaussian profiles and do not have the more characteristic flat-topped or doubled-lobed properties seen at shorter wavelengths. This is probably due to the lower resolution of the spectrum, which only partially resolves the lines.

Owing to their weakness and low expected fluxes, the identifications of some of the higher lying transitions with their larger quantum numbers are somewhat in doubt. Additionally, several other lines from different transitions fall within the Doppler widths (0.15 μm or about 4500 km s^{-1}) of the lines, and therefore their relative contributions are uncertain unless Case B conditions are assumed (Case B assumes that every Lyman photon is scattered many times before being converted to a Lyα photon plus a higher series photon, the latter of which escape the shell without further scattering). For example, Pfα (6–5) at 7.4598 μm is blended with Huβ (8–6) at 7.5025 μm and other H I lines at 7.5081 μm (11–7) and 7.4951 μm (17–8). Similarly, Huα (7–6) at 12.3719 μm is contaminated by H I (11–8) at 12.3872 μm.

On September 7, the [Ne II] line at 12.81 μm was clearly seen, indicating a thinning ejecta shell and a possibly hardening radiation field. The line profile was not Gaussian and showed evidence of being flat-topped or double-peaked. A close examination of the August 11 spectrum reveals a weak, double-peaked feature at a wavelength that is approximately 0.02 μm longer than the [Ne II] line on September 7. No known H I line falls at this wavelength for an upper level <20, so this may be the early appearance of [Ne II]. The [Ne II] line in novae is usually, but not always, associated with ONeMg WDs. In this case, however, we believe that this nova originated on an ONeMg WD because of the [Ne II] 12.8 μm line, the optical [Ne III] line, and the speed of the nova.

Three lines remain unidentified: 7.675, 8.425, and 9.047 μm. Unlike the H I lines, these features grew stronger with time. Their wavelengths do not coincide with any H I line whose upper level is less than 20, although H I (21–9) falls at 9.044 μm. Higher upper levels with their larger ΔN values seem unlikely. These are most likely neutral metal lines or first ionization levels of elements with low ionization potentials because they increase in strength with time. The strengths of molecules would be expected to decrease in strength with time, because the hardening radiation field tends to dissociate them and the decreasing density makes formation less likely.

5. NEAR-IR SPECTRA (DAYS 10–58)

The sequence of observations of V1187 Sco in the near-infrared is one of the most, if not the most, complete in detailing

TABLE 2
MICHELLE/GEMINI LINE LIST

Wavelength (vacuum) (μm)	ID	2004 Aug 11 Line Flux (W cm^{-2})	2004 Sep 7 Line Flux (W cm^{-2})	2004 Sep 26 Line Flux (W cm^{-2})	Comments
7.4598	H I 6–5	6.33E−18	1.71E−18	3.74E−19	Blended with H I 17–8 7.495 μm, 8–6 7.502 μm, 11–7 7.508 μm
7.675	?				
7.7804	H I 16–8	1.14E−19	9.20E−20		
8.1549	H I 15–8	1.35E−19	2.94E−20	6.05E−21	
8.425[a]	?	2.61E−20		3.10E−21	
8.665	H I 14–8				
8.76	H I 10–7	7.69E−19	1.76E−19	9.33E−21	
9.047[a]	?	1.80E−20	1.22E−20	6.07E−21	
9.392	H I 13–8	1.49E−19	8.66E−21		
9.522	H I 19–9				In ozone, too confused to measure
9.66		Blend	1.00E−19		In ozone, too confused to measure
9.847	H I 18–9	5.53E−20			In ozone, too confused to measure
10.2613	H I 17–9	6.82E−20	2.01E−20		
10.5035	H I 12–8	2.52E−19	7.19E−20	6.06E−21	
10.8036	H I 16–9	7.32E−20	2.54E−20		
11.3087	H I 9–7	6.64E−19	1.70E−19	1.08E−20	
11.5395	H I 15–9	1.10E−19	2.33E−20	2.44E−21	
12.3719	H I 7–6	1.90E−18	5.26E−19	3.46E−20	Blended with H I 11–8 12.3833 μm
12.387	H I 11–8				
12.5871	H I 14–9	1.69E−19			
12.8135	[Ne II]		1.01E−19	7.65E−21	
13.188	H I 18–10	Cut off			

[a] Measured wavelength for unidentified lines.

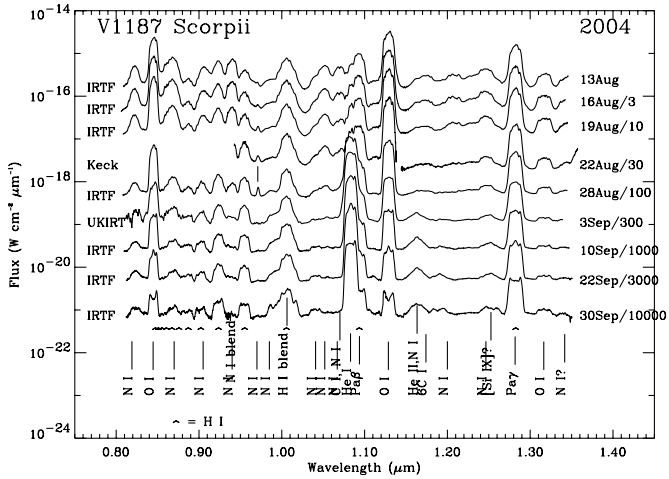

FIG. 5.—SPEX, CGS4, and NIRSPEC data time sequence in the 0.8–1.4 μm region. The spectra have been multiplied as indicated in the legend to separate them for clarity. Note that this plot is logarithmic in flux. The H I lines are indicated by chevrons. Many lines appear, disappear, grow, and change. Several lines remain unidentified.

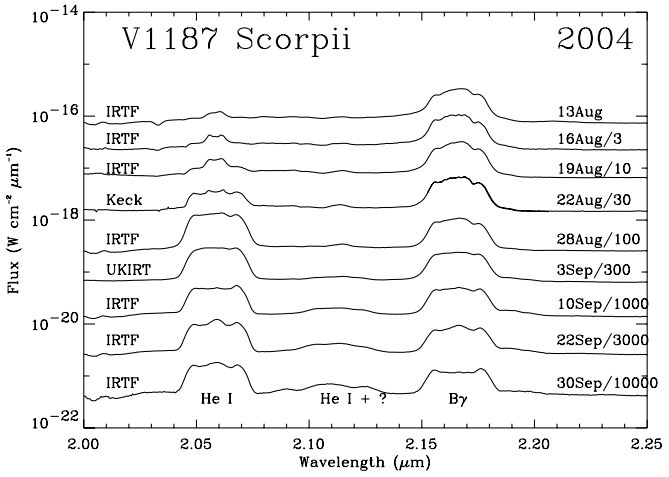

FIG. 7.—Time evolution of the He I 2.0581 μm and H I Brγ 2.1655 μm. Paγ decreases in strength and develops spectral structure, eventually showing a flat-topped profile with a central peak that disappears leaving a doubled-peaked profile. The helium line begins as a narrow, doubled-peaked emission line, then grows rapidly in strength, and broadens into a flat-topped profile with some weak structure.

the time development of an ONeMg nova at these wavelengths. While the development was generally a steady process dictated by the rise in excitation, there were a few unexpected aspects, namely the persistence of certain low-excitation lines (most notably those of O I), and the general weakness of coronal lines with the exception of those of sulfur.

Figures 5 and 6, respectively, show the 0.8–1.4 and 1.4–2.5 μm portions of the nine spectra that span the dates from August 13 to September 30. The three earliest spectra were dominated by the O I lines at 0.8446 and 1.1287 μm, that, together with O I 1.3165 μm are used to derive the reddening in § 8. The first two lines are produced mainly by fluorescence by Lyβ (Bowen 1947). Their strengths indicate that the regions in which they arose must not only be thick to Lyβ, but to Hα as well. H I $n = 3$ can decay to Lyα and Hα, and if Hα is not optically thick, this process will drain the Lyβ much more efficiently than conversion to O I (Grandi 1980). This indicates that Case B conditions within these regions (optically thick resonance lines, optically

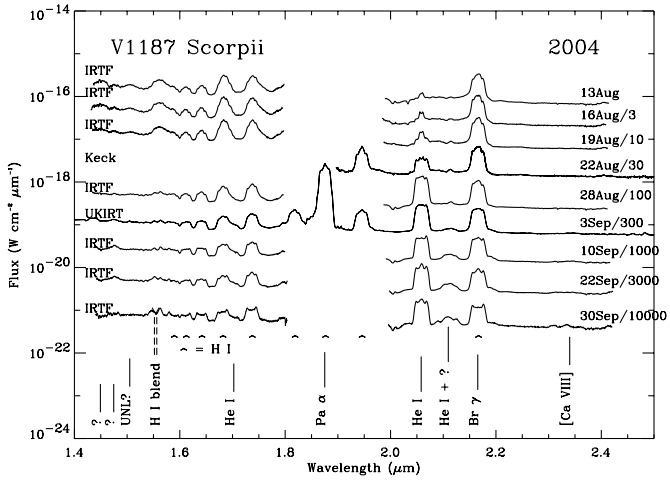

FIG. 6.—SPEX, CGS4, and NIRSPEC data time sequence in the 1.4–2.6 μm region. The spectra have been multiplied as indicated in the legend to separate them for clarity. Note that this plot is logarithmic in flux. The H I lines are indicated by chevrons. Many lines appear, disappear, grow, and change. Of particular note is the emergence of the [Ca VIII] coronal line at 2.32 μm. Several lines remain unidentified.

thin subordinate lines) were not met for the H I lines, and thus their ratios could not be predicted from simple recombination theory. Note that because of the persistence of the O I lines, this was true for the later data as well.

Lines of O I and H I dominated the early spectra, but as frequently happens, the He I 1.0830 and 2.0581 μm lines quickly strengthened and ultimately became the strongest emission features except for Paα 1.875 μm, which is only occasionally of use because of its location within a strong terrestrial water vapor band (see UKIRT spectrum in Fig. 6). Lines of neutral nitrogen were numerous and strong in the early epochs. With the exception of the [N I] features around 1.04 μm, these are all permitted features and formed by recombination. Their unusual strength was probably due to the size of the warm, low-excitation regions (that also gave rise to the O I lines) and an overabundance of nitrogen. In this sense they were very similar to the prominent N I lines produced by novae from systems with CO WDs. In contrast, the C I lines seen at early epochs in CO systems (e.g., V2274 Cyg = Nova Cyg 2001 No. 1; Rudy et al. 2003) were not present at anything near comparable strength in V1187 Sco. Whether this is generally true of ONeMg systems will require observations of additional systems. If true, it could provide a means for nova classification from infrared spectra alone. Similarly, Fe II features were not readily detectable in the early near-infrared spectra of V1187 Sco. While this was in part due to masking by strong, nearby emission lines, they were clearly not present at the level seen in CO novae like V2540 Oph (Rudy et al. 2002a). These facts also lend support the classification of V1187 Sco as an ONeMg nova.

By the end of August, V1187 Sco had progressed to an intermediate stage of excitation. This was indicated by the general weakening of the features from neutral metals and the emergence of the He I 1.0830 μm line as the strongest feature. Recombinations and collisional excitation from its metastable lower level ($2\ ^3S$) account for its great strength. Its profile is compared to a companion singlet feature (He I 2.0581 μm) in Figures 7 and 8. Between August 28 and September 3, the He II features emerged rapidly, marking the appearance of the higher excitation emission lines.

About the same time as the He II lines become detectable, the coronal lines [S VIII] 0.9911 μm and [S IX] 1.2520 μm appeared.

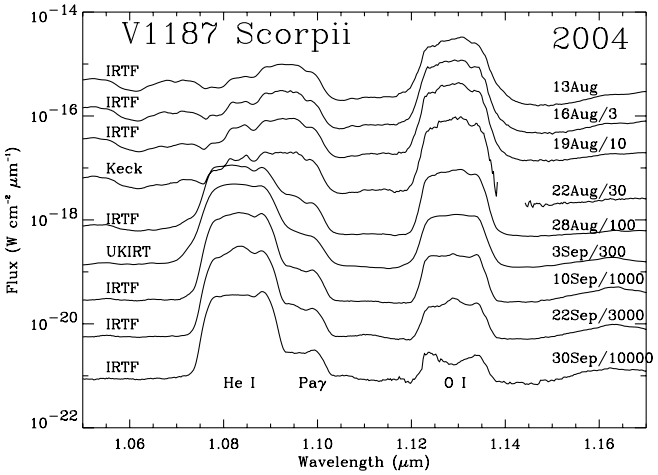

FIG. 8.—Time evolution of the He I 1.0830 μm and H I Paγ 2.1655 μm. The time evolution is similar to that shown in Fig. 7.

The former was blended with Paδ, while the latter was masked by N I lines that gradually declined as it strengthened. [S IX] 1.2520 μm was recognizable as a high-excitation line, as opposed to an N I feature or He I 1.2528 μm, from the triangular profile it shared with the He II lines (see the 5–7 transition at 1.1626 μm).

Also appearing along with the He II and coronal lines were features at 1.1110, 1.1900, 1.5545, and 2.0996 μm, four of the six so-called unidentified novae lines (UNL) frequently seen in novae. They are common in the later stages of both CO and ONeMg systems (e.g., Williams et al. 1996; Lynch et al. 2001). Accurate wavelengths for the UNL were first measured in the comparatively narrow-lined nova V723 Cas (Nova Cas 1995) by Rudy et al. (2002b). Note that the UNL observed here shared the distinctive triangular profiles of the He II and coronal lines during the September 19 and 22 measurements, possibly confirming their high-excitation nature.

In the last measurement on September 30, the frequently seen coronal lines [Si VI] 1.9645 μm and [Ca VIII] 2.3205 μm were present. Although the weakness of these features relative to [S VIII] 0.9911 μm and [S IX] 1.2520 μm may have other causes, a possible explanation is that the sulfur abundance is significantly enhanced. At this epoch, the profiles of the coronal lines and the unidentified features had changed from the triangular profiles of

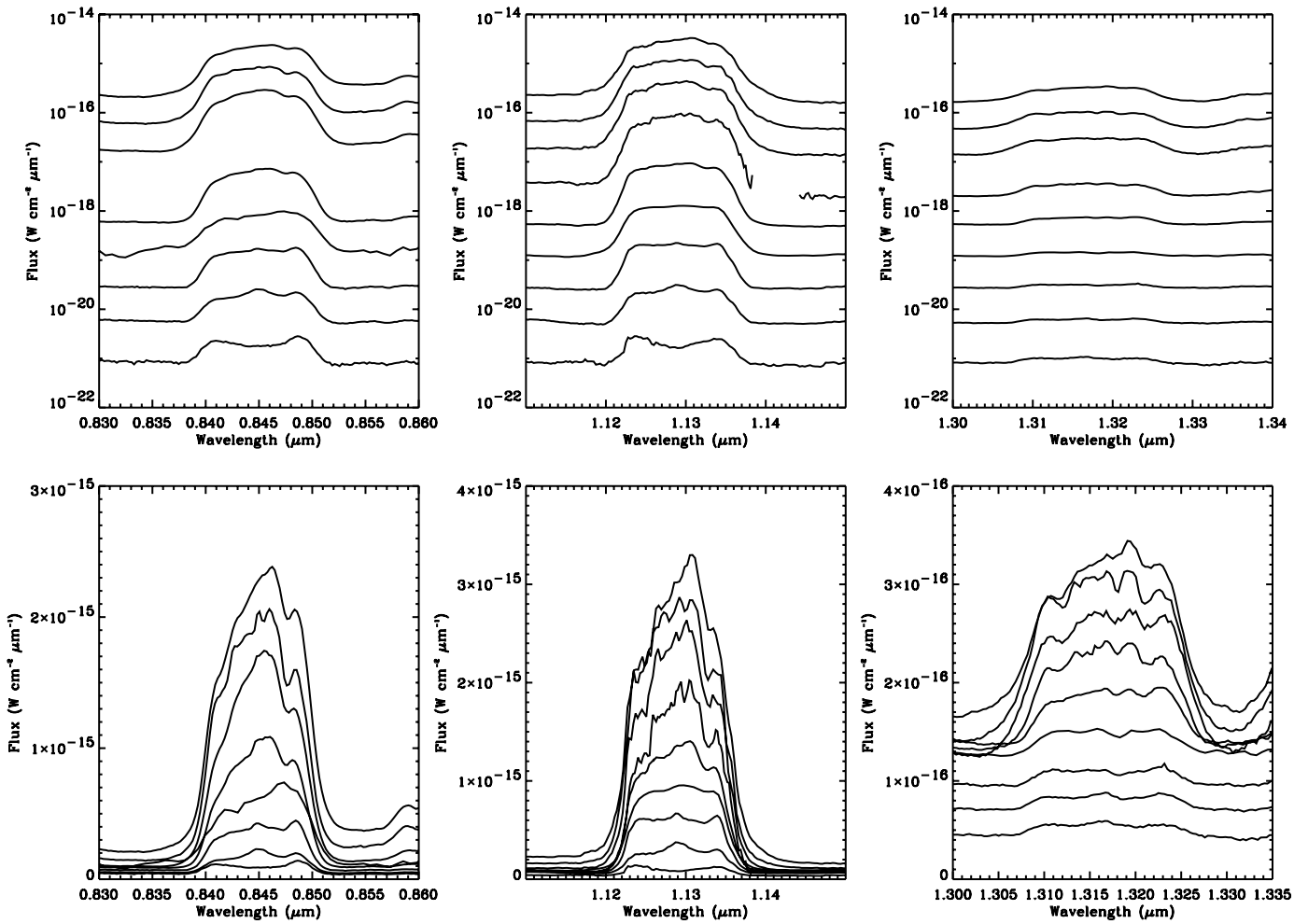

FIG. 9.—O I line profile evolution. The O I lines at 0.8446, 1.1287, and 1.3164 μm are plotted here, logarithmic on top with the same scaling factors as Fig. 8 and linear on the bottom. The scaling on the bottom is arbitrary and designed to show the structure. Time evolution is downward, with the earliest spectrum on top and latest on the bottom. In view of the way the lines form, as cascades from Lyβ and Lyman continuum fluorescence, their similarity in shape is not surprising. The spectral structure probably reflects Doppler-shifted density inhomogeneities.

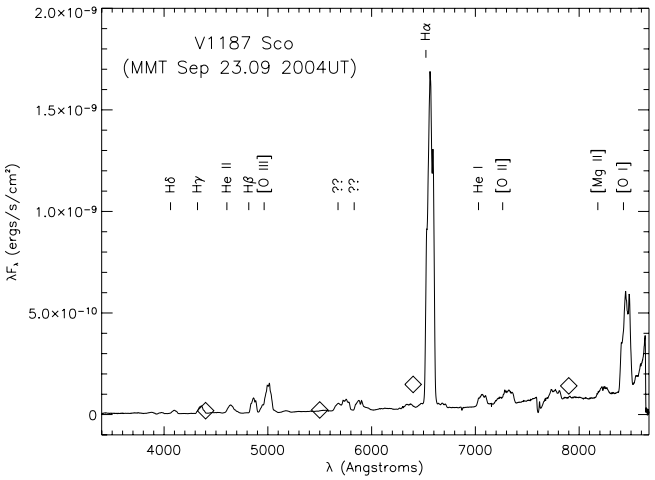

Fig. 10*a*

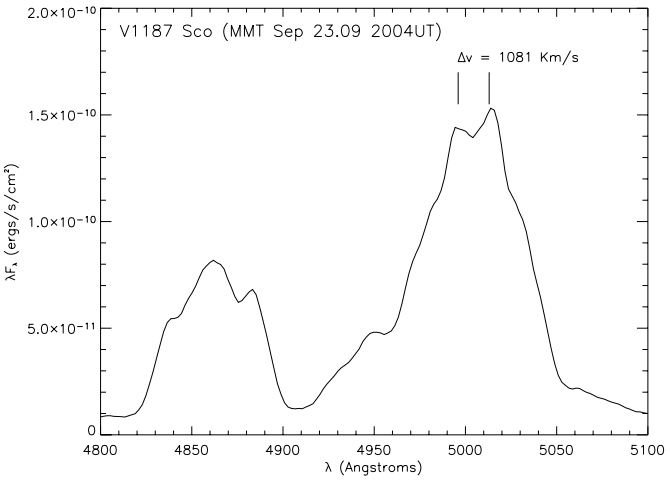

Fig. 10*b*

Fig. 10.—(*a*) 0.33–0.87 μm optical spectrum from the MMT 51 days after maximum brightness. The diamonds are optical photometry obtained by Zamanov et al. (2004) on 2004 September 26.836 UT. Note the absence of both [O I] $\lambda\lambda$6300, 6363 and He II λ4686. (*b*) Enlargement of the spectrum from (*a*) near the [O I] λ5007 line illustrating the double-peaked profile typical of most emission lines at this epoch. The velocity components are separated by approximately 1200 km s^{-1}, and the line profiles may be attributed to a ringlike (slow) and spherical shell (fast) admixture of expelled material (see § 11).

a week earlier to the flat-topped or saddle-shaped shapes of the lower excitation lines. Finally, we note that the presence of [S IX] 1.2520 μm together with the absence of [S XI] 1.9196 μm implied that the most energetic photons had energies between 329 and 447 eV.

The He I lines at 1.0830 and 2.0581 μm were particularly interesting. Both have metastable lower levels and are collisionally excited. Although the two lines evolved in slightly different ways—probably as a result of different optical depths—their behavior followed a similar path. Referring to the 2.0581 μm line (Fig. 7), the earliest observation on August 13 (day 10) revealed a narrow emission line with evidence of doubling with components at $\pm$300 km s^{-1}. Three days later the doubling was clearly evident with two separate components at $\pm$400 km s^{-1}. Both spectra showed a hint of broad, doubled emission around $\pm$1300 km s^{-1} that was confirmed on the night of August 19 when the broad component strengthened significantly. By mid-September a strong central emission feature appeared in the He I lines and remained to the end of the observation period. The He I 1.0830 μm line showed essentially identical behavior (Fig. 8).

The CNO lines are always of interest in novae because a TNR on an ONeMg WD always includes CNO reactions. V1187 Sco showed many emission lines of all three neutral elements. Most classical novae show many N I and C I emission lines in the infrared because nitrogen is always enhanced regardless of WD type (Schwarz et al. 2001; Schwarz 2002; Vanlandingham et al. 1996, 1997, 1999, 2005). The Lyβ-fluoresced O I lines were very strong throughout the observing period (Fig. 9) and showed a number of line profile changes.

In the 0.8–2.5 μm region, V1187 Sco's spectrum on September 3 (day 31) closely resembled that of V4741 Sgr on its day 95 (Mazuk et al. 2002), another novae we believe to be an ONeMg nova. The same lines are present, and they generally had the same relative strengths.

6. OPTICAL SPECTRUM (DAY 51)

The optical spectrum in Figures 10*a* and 10*b* revealed a wealth of neutral and singly ionized lines and a number of forbidden lines (Table 3). At this stage, the ejecta were being illuminated by a much hotter WD than before, and the higher excitation level was shown by lines of He II, [Fe VI], N III, and [Ne III]. The redward upslope of the continuum is a result of high extinction (see §§ 8 and 9).

Previous studies (Shore et al. 2003; G. J. Schwarz et al. 2006, in preparation) have shown that there is a remarkable consistency in the spectral development of novae, particularly among ONeMg novae. This pattern also holds with V1187 Sco. Figure 11 compares the optical spectrum of V1187 Sco (*solid lines*) with two

TABLE 3
MMT Line List: 2004 September 23 UT

Wavelength[a] (Å)	ID	Flux (W cm^{-2})
3870	[Ne III] λ3874	5.20E−21
3889	H8	2.40E−21
3976	[Ne III] λ3971+Hε	5.60E−21
4101	Hδ	1.90E−20
4340	Hγ	1.90E−20
4366	[O III] λ4363	2.60E−20
4639	N III λ4640	4.50E−20
4680	He II λ4686)	1.30E−20
4865	Hβ	7.90E−20
4964	[O III] λ4959	3.60E−20
5010	[O III] λ5007	1.60E−19
5176	[Fe VI] λ5176	9.50E−21
5679	N II λ5679	4.40E−20
5755	[N II] λ5754	6.90E−20
5879	He I λ5876[b]	6.50E−20
5948	?	1.80E−20
6358	?	2.80E−20
6568	Hα	1.60E−18
7070	He I λ7065	6.40E−20
7237	C II λ7234?	3.10E−20
7320	[O II] λ7325	8.80E−20
7771	O I λ7773	5.20E−20
8235	Mg II λ8232?	6.10E−20
8445	O I λ8446	4.40E−19

[a] Observed or deblended wavelength.
[b] Lower limit due to strong interstellar Na I $\lambda\lambda$5890, 5896 absorption.

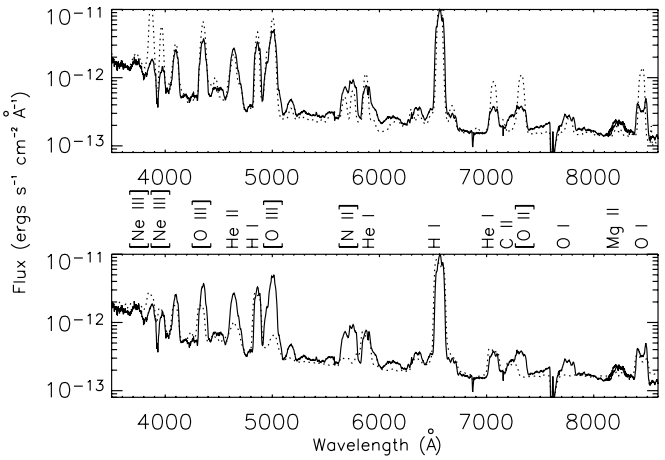

FIG. 11.—Comparison of the scaled, optical spectra of V1187 Sco and the fast nova V1974 Cyg (*top*) and the very fast nova V838 Her (*bottom*). V1187 Sco is the solid line in both panels. The spectra were obtained at similar points of their spectral evolutions and show many similarities. The differences are due primarily to each nova's distinctive mass distribution and elemental abundance.

other well-observed ONeMg novae (*dotted lines*) at similar points of their spectral evolutions. In the top panel the comparison is with the slower nova V1974 Cyg, $t_2 = 17$ days, obtained approximately 82 days after visual maximum (Austin et al. 1996). The bottom panel shows optical spectrum taken about 10 days after visual maximum of the extremely fast nova V838 Her, $t_2 = 2$ days (Vanlandingham et al. 1996). This comparison provides some insight into the abundances of V1187 Sco relative to these other novae (G. J. Schwarz et al. 2006, in preparation). For example, the more pronounced lines of oxygen and nitrogen in V1187 Sco relative to V838 Her may indicate that V1187 Sco has a greater enhancement of these elements. However, these general impressions must still be confirmed through a rigorous abundance analysis that will be presented in a later paper from data obtained when the nova reaches its full nebular phase.

Shore et al. (2003) found that the similarities in the time-scaled optical spectra of ONeMg nova were also valid in the ultraviolet. The large set of early observations in this study allows us to confirm the same trend in the infrared. The time at

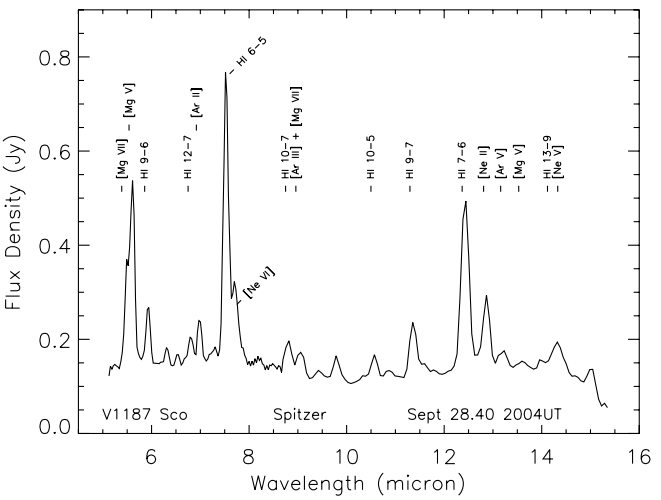

FIG. 12.—*Spitzer* IRS spectra data: IRS Short-Low spectrum (channel 0). Line-of-sight background has been removed by differencing spectra obtained at two nod positions along the long slit (see § 2 for a discussion).

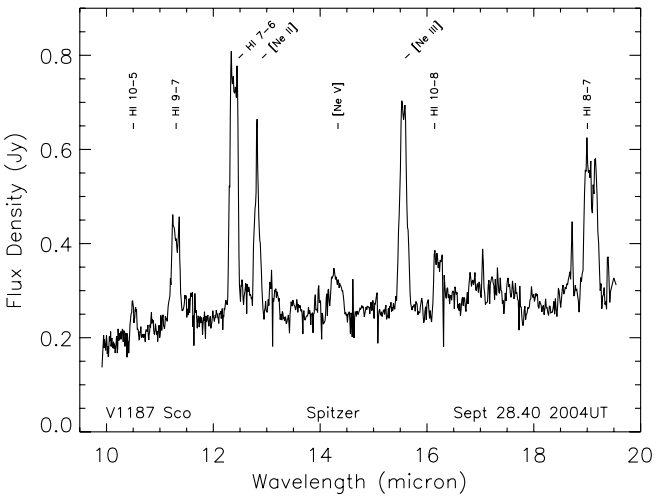

FIG. 13.—*Spitzer* IRS spectral data: IRS Short-High (channel 1). No background has been removed, as was done in Fig. 12.

which the He I 2.0581 μm flux equals that of Brγ is one such diagnostic. In V1187 Sco this happens between the observations taken on August 22 and 28, or 19–25 days after outburst. The same occurs in V838 Her (Harrison & Stringfellow 1994) and V1974 Cyg (Woodward et al. 1995) about 5 days and less than 64 days after their respective maxima. These dates scale very well with the observed t_2 decay times and show that the spectral development of novae are similar over a wide range of wavelengths.

7. *SPITZER* SPECTRA (DAY 56)

Figures 12–14 show the spectra taken by *Spitzer* on 2004 September 28. By this time the nova had entered the early coronal phase. Figure 12 shows emission lines of [Mg V], [Mg VII], [Ne V], and [Ar V], although residual H I recombination emission lines were still the strongest in the spectrum. Figure 13 shows a range of forbidden Ne lines and strong H I emission. The spectral resolution in Figure 13 is high enough to reveal the flat-topped or slightly doubled line profiles like those seen at shorter wavelengths. Figure 14 is a bit noisy, and the only line that stands out is

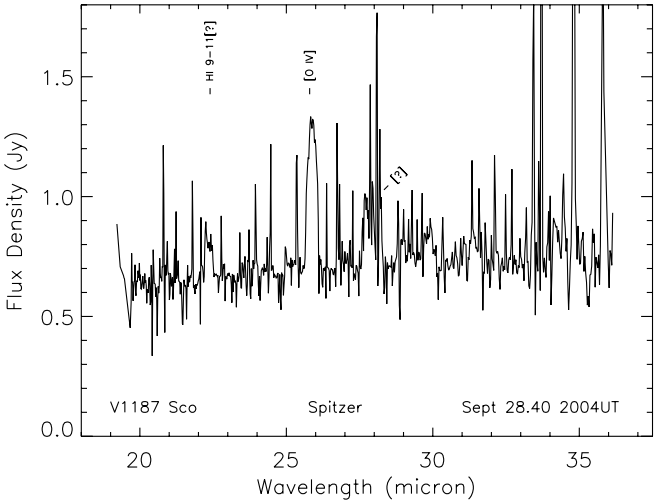

FIG. 14.—*Spitzer* IRS spectral data: IRS Long-High (channel 3). No background has been removed, and narrow line-of-sight interstellar emission lines are evident.

TABLE 4
Spitzer Lines

Tentative Line ID	Vacuum Wavelength (μm)	Flux (W cm^{-2})	Error Flux (W cm^{-2})
?.....		3.719E−20	1.308E−20
[Mg VII].....	5.5032	2.435E−19	3.593E−20
[Mg V].....	5.6099	4.118E−19	2.479E−20
H I 9–6.....	5.9082	1.205E−19	1.111E−20
H I 13–7.....	6.2919	4.281E−20	1.015E−20
[Si VII]	6.4922	2.303E−20	9.847E−21
H I 12–7.....	6.7719	5.009E−20	1.136E−20
[Ar II].....	6.9853	8.257E−20	1.867E−20
H I 6–5.....	7.4600	4.098E−19	3.944E−21
[Ne VI].....	7.6524	8.337E−20	6.040E−21
H I 10–7.....	8.7600	3.219E−20	5.032E−21
[Ar III].....	8.9910	1.866E−20	5.293E−21
H I 12–8.....	10.5035	1.450E−20	2.620E−21
H I 9–7.....	11.3087	2.958E−20	4.071E−21
H I 7–6.....	12.3719	8.535E−20	1.195E−21
[Ne II].....	12.8136	2.764E−20	2.291E−21
[Ar III].....	13.1000	1.008E−20	2.247E−21
[Ar III]?.....	13.5400	4.214E−21	1.435E−21
H I 13–9.....	14.1831	9.880E−21	2.254E−21
[Ne V]?.....	14.3200	8.837E−21	1.977E−21

Note.—Lines fit with FWHM = 0.1185 μm.

[O IV] at 25.89 μm. Table 4 lists the lines and line fluxes from the spectrum.

8. REDDENING, EXTINCTION, AND DISTANCE

As in past studies of novae (e.g., Rossano et al. 1994; Rudy et al. 2003; Venturini et al. 2004; Lynch et al. 2004), we use the fluorescently excited lines of neutral oxygen to estimate the reddening for V1187 Sco. This procedure, first described by Rudy et al. (1991), uses the O I λ8446 and λ11287 lines that are produced in equal photon numbers through the decay of a resonant transition coincident with H I Lyβ (Bowen 1947). Corrections to the intrinsic line ratios for continuum fluorescence, which does not generate O I λ8446 and λ11287 in equal amounts, are made from the strength of O I λ13164. Seven independent observations of all three of these O I features were made over a period of approximately 50 days. Because V1187 Sco did not form dust during this period, the reddening should have been solely interstellar in origin and thus nonvariable. In fact, this is exactly what we found. Although the intensities of the O I lines declined by as much as a factor of 200 during this period, the derived reddening values are identical within the measurement uncertainties. The high and low values are $E(B-V) = 1.71$ and 1.47, respectively. The average value and the standard deviation of the seven measurements are $E(B-V) = 1.56 \pm 0.08$. Assuming that $A_V/E(B-V) = 3.0$, we find $A_V = 4.68 \pm 0.24$.

An independent estimate of the reddening can be derived from the optical spectrum based on the work of Munari & Zwitter (1997), who provided a robust way to estimate $E(B-V)$ from the Na I D equivalent widths. The doublet lines ($\lambda\lambda$5890, 5896) are strong resonance transitions and are clearly observed in our September 23 optical spectrum. The measured Na D1+D2 equivalent width is about 3 Å, resulting in a D1 equivalent width between 1.6 and 2 Å. Based on Figure 4 in Munari & Zwitter (1997), we estimate $E(B-V) = 1.2$–1.5, consistent with the value derived above from the O I line ratios.

Another approach to estimate the reddening to V1187 Sco is to use the information available on photographic plates obtained prior to outburst, since Szkody (1994) showed that old novae have $(B-V)$ values clustered around zero. Assuming that the V1187 Sco precursor had an intrinsic $(B-V)$ color of zero, the USNO-A2.0 blue and red plates can provide the observed quiescent color information. M. R. Kidger provides unpublished transformations from USNO-A2.0 red and blue plate magnitude to Landolt *BVR* magnitudes.[23] The transformations are based on comparisons of USNO-A2.0 and Landolt calibrated standard stars from four fields in Gonzalez-Perez et al. (2001). The $E(B-V)$ derived from this method was 1.3, which, again, is consistent with our previous determinations.

With a well-defined reddening obtained using the O I lines, we can calculate the distance by using the various relations between absolute visual magnitude at peak brightness and rates of decline, or absolute visual magnitude 15 days after maximum (Schmidt 1957; Cohen 1985; Capaccioli et al. 1989; van den Bergh & Younger 1987). Using m_V (peak) and m_V (+15 days) of 9.7 and 12.7, respectively, and the previously quoted values for A_V, t_2, and t_3, we find the distance to be $D = 4.9 \pm 0.5$ kpc, our most reliable distance estimate.

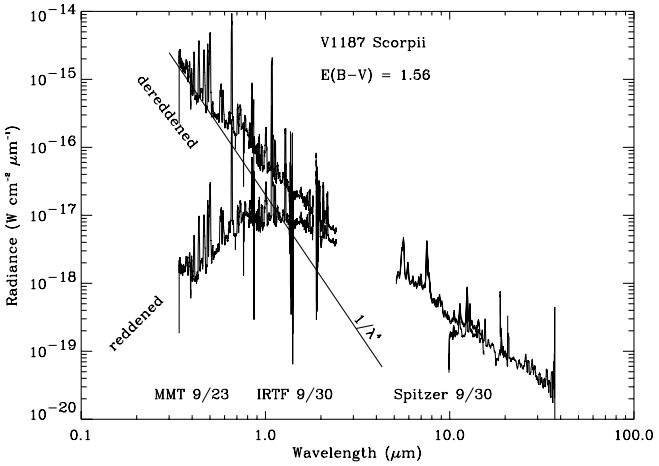

Fig. 15.—Spectral energy distribution constructed by combining nearly time-coincident spectra from the MMT (September 9), IRTF (September 30), and *Spitzer* (September 28). It is dominated by interstellar reddening. When dereddened, the spectrum shows a monotonic decline to the red with a slope slightly lower than that of a Rayleigh-Jeans spectrum ($1/\lambda^4$).

9. SPECTRAL ENERGY DISTRIBUTION (SED)

Using data from the MMT, IRTF, and *Spitzer* taken within a few days of each other, we have assembled a spectral energy distribution (SED) for late 2004 September (Fig. 15). The arched continuum structure of the unreddened spectrum is a result of the high extinction. To deredden the spectrum, we took the value of $E(B-V)$ determined from the O I line ratios and applied the reddening curves of Savage & Mathis (1979) and Draine (1989). We assumed that the reddening was all interstellar in origin, which was probably the case since V 1187 Sco did not manifest any evidence of local dust formation. When dereddened, the spectrum decreased monotonically toward longer wavelengths, although slightly less steeply than a Rayleigh-Jeans spectrum. This shape is consistent with the often-mentioned F-type optical continuum that novae show near maximum.

10. LINE STRENGTHS AND PROFILES

V1187 Sco's infrared spectra displayed a wide range of line profiles and, perhaps more importantly, significant profile changes

[23] See http://www.iac.es/galeria/mrk/comets/USNO_Landolt.htm.

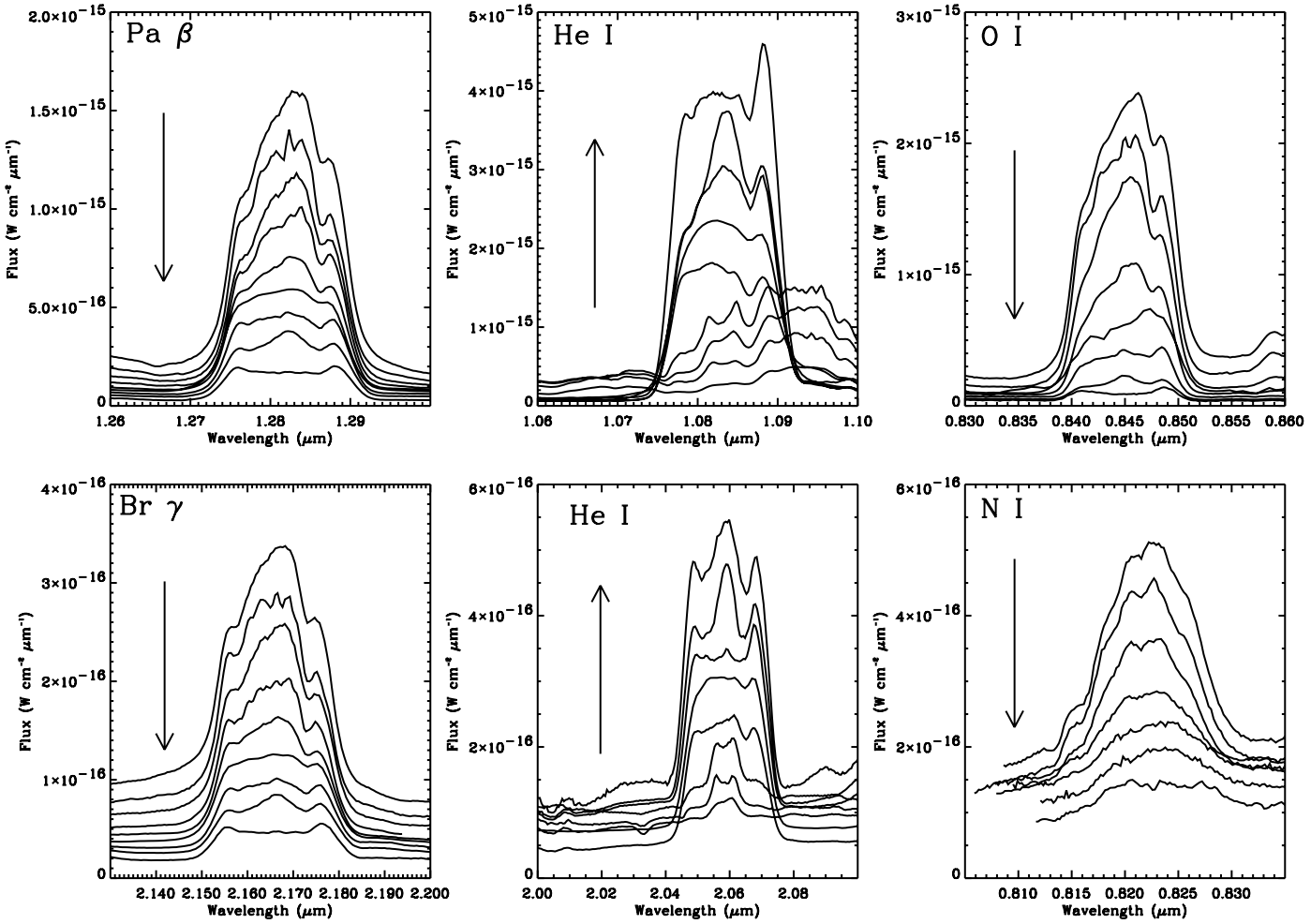

FIG. 16.—Evolution of a variety of strong lines: Paβ, He I 1.0830 μm, O I 0.8446 μm, Brγ, He I 2.0581 μm, and N I 0.823 μm. The arrow shows the direction of time. There appears to be some Doppler structure common to all species, and at the same time, large differences in structure within the broad Doppler widths that are probably due in part to density inhomogeneities. While the overall widths did not change appreciably, the structure in the lines did.

with time and significant profile differences from one atomic species to another. Figure 16 shows the evolution of a variety of strong lines: Paβ, He I 2.0581 μm, O I 0.8446 μm, Brγ, He I 2.0581 μm, and N I 0.823 μm. There appears to be some Doppler structure common to all species, and at the same time, large differences in structure within the broad Doppler widths that is probably due in part to density inhomogeneities. While the overall widths did not change appreciably, the line profiles did. Since the initial ejection speed must be well above escape velocity (a few thousand kilometers per second), the continuing changes in the line profiles may be due to the modulation of wind close to the binary system (Lynch et al. 2002).

It is likely that the strongest H I lines were optically thick during much, if not all, of the observation period, and they were almost certainly thick in the early day of the outburst. Not only would saturation affect the line shapes, but only the near side of the ejecta or the near side of the far blobs from the ejecta would contribute to the line emission. The other species, with the possible exception of He I, were almost certainly optically thin and therefore representative of the entire ejected mass. Therefore, any systematic variations among species should be due to the different excitation energies and the location of the species relative to the WD, e.g., closer in, farther out, etc.

Figure 17 shows some of the line fluxes from Table 5 as a function time. The low-excitation neutral species appeared first,

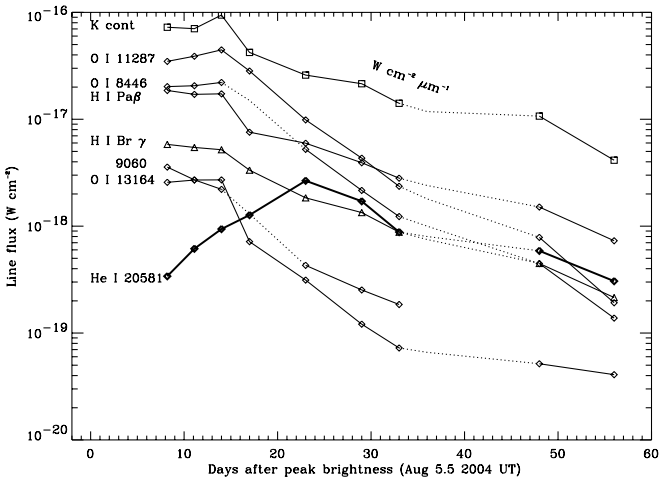

FIG. 17.—Line fluxes vs. time. The low-excitation neutral species appeared first, initially grew in strength, before reaching a maximum about 15 days after the outburst, and then decreased monotonically. The higher excitation neutral species of He I started out weak even at maximum light and only later reached their maximum, in this case about 23 days after peak brightness.

TABLE 5

LINE FLUXES

Line ID	λ (μm)	Aug 13 (W cm^{-2})	Aug 16 (W cm^{-2})	Aug 19 (W cm^{-2})	Aug 22 (W cm^{-2})	Aug 28 (W cm^{-2})	Sep 3 (W cm^{-2})	Sep 10 (W cm^{-2})	Sep 22 (W cm^{-2})	Sep 30 (W cm^{-2})
					Single Lines					
H I Pa11	0.8863	3.65154E−19	4.18848E−19	4.46676E−19				1.0583032E−19	9.2158384E−20	3.248605E−20
H I Pa10	0.9015								1.0139E−19	5.7938998E−20
H I Pa9	0.9229	5.4326054E−18	4.3795741E−18	3.7653082E−18		1.0514673E−18	5.3317081E−19	4.9898186E−19		
H I Pa8	0.9545	2.3071629E−18	2.0288495E−18	2.0732369E−18	1.36367E−18	7.7013707E−19	4.3014763E−19	4.4393546E−19	2.2522838E−19	8.71577E−20
N I	0.9708	5.03814E−20	7.04283E−20	1.31304E−19	1.10966E−19	8.02254E−20				
[S VIII]	0.9913									
[N I]	1.04								5.83494E−20	2.6798E−20
He I	1.083									
H I Paγ	1.0938								1.18589E−20	
O I	1.1287	3.48327E−17	3.89189E−17	4.4628E−17	2.83092E−17	9.86909E−18				
He II	1.1626						2.60394E−19	3.47148E−19	2.1000383E−19	1.3825994E−19
UNL	1.1901								7.8100164E−20	6.1974882E−20
N I	1.2461	6.1784492E−18	5.545459E−18	5.3417681E−18	4.46662E−19	3.71011E−19				
[Si IX]	1.252									6.43605E−20
H I Paβ	1.2818	1.86452E−17	1.71319E−17	1.72995E−17	7.57255E−18	5.96962E−18		2.81395E−18	1.50567E−18	7.29587E−19
O I	1.3165	2.5695E−18	2.70126E−18	2.70565E−18	7.16252E−19	3.13476E−19	1.20534E−19	7.25169E−20	5.15794E−20	4.07903E−20
N I	1.343									
N I	1.3582	1.0784E−17	1.19455E−17			5.98121E−19				
He II	1.476							1.46603E−19	8.3496998E−20	
Mg I ?	1.5025	1.1283163E−18	8.0137048E−19	9.8956977E−20						
UNL	1.5545									
H I Br14	1.5881									
H I Br13	1.6109	6.15667E−19	5.5733E−19	5.87396E−19		2.27387E−19	1.42292E−19	1.10342E−19	5.09443E−20	2.59318E−20
H I Br12	1.6407	1.02614E−18	9.66943E−19	9.8116E−19		3.71007E−19	2.36579E−19	1.65629E−19	9.13836E−20	4.65462E−20
H I Br11	1.6806	3.82903E−18	3.6881E−18	3.57723E−18		9.09438E−19				
He I	1.7002									
H I Br10	1.7362		3.68294E−18	3.51026E−18		1.09195E−18	6.07697E−19	4.1487E−19	2.50089E−19	1.22317E−19
H I Br9	1.8174						8.04363E−19			
H I Paα	1.8751				4.18994E−17		1.45894E−17			
H I Br8	1.9446				2.7085387E−18		9.67934E−19			
[SI VI]	1.9641									
He II ?	2.0373									
He I	2.0581	3.39747E−19	6.15302E−19	9.40486E−19	1.27268E−18	2.65876E−18	1.70781E−18	8.81279E−19		3.05887E−19
He I	2.1132	3.99603E−20	6.1901966E−20	7.91095E−20	5.79187E−20	4.56829E−20				
H I Brγ	2.1655	5.82368E−18	5.45144E−18	5.18673E−18	3.34271E−18	1.83806E−18	1.34351E−18	8.78653E−19	4.48059E−19	2.14572E−19
[Ca VIII]	2.3214								2.90636E−20	2.94066E−20

TABLE 5—*Continued*

Line ID	λ (μm)	Aug 13 (W cm^{-2})	Aug 16 (W cm^{-2})	Aug 19 (W cm^{-2})	Aug 22 (W cm^{-2})	Aug 28 (W cm^{-2})	Sep 3 (W cm^{-2})	Sep 10 (W cm^{-2})	Sep 22 (W cm^{-2})	Sep 30 (W cm^{-2})
					Groups and Blends					
N I	0.8188–0.8242	2.9345082E−18	2.5761468E−18	1.8682657E−18		4.1611E−19				
H I Pa18, O I, H I Pa17	0.8438, 0.8446, 0.8467	2.0182253E−17	2.0598856E−17	2.2060191E−17		5.23276E−18	2.1618834E−18	1.23455E−18	4.47028E−19	1.3781E−19
H I Pa13, N I	0.8665, 0.8629–0.8629									
N I	0.8680–0.8711									
C I	0.9061–0.9112	3.5737754E−18	2.7075006E−18	2.0400384E−18						
N I, C I	0.9362–0.9461,0.9406	6.2428382E−18	5.4832628E−18	4.038832E−18		4.2251507E−19				
N I ?	0.9823–0.9883				8.84759E−20					
H I Paδ, He II	1.0049, 1.0124				4.00221E−18					
N I	1.0507–1.0550					4.9525769E−19				
C I	1.0683–1.0754	4.3373368E−18	2.351774E−18							
UNL, O I	1.1114, 1.1287						4.33447E−18	2.36453E−18	7.84834E−19	1.91715E−19
He II, C I	1.1626, 1.1600–1.1674									
C I	1.1748–1.1823									
UNL, He I	1.1901, 1.1969									
N I	1.1969–1.2187	3.6340978E−18	3.4393652E−18	3.050356E−18						
He I, H I Paβ	1.279, 1.2818						3.92253E−18			
N I	1.3582–1.3588									
C I	1.4420–1.4472	2.5856819E−18	1.8323967E−18	1.2996448E−18						
C I	1.4738–1.4852	8.8972234E−19	7.8707788E−19							
UNL, H I Br16	1.5545, 1.5557									
UNL, He I	2.0996, 2.1120						6.7148E−20	1.19187E−19	1.1352E−19	6.77704E−20
He II, [TI VII]?	2.1885, 2.2050									
He II, [Ca VIII]	2.3463, 2.3214									

NOTES.—UNL = Unidentified nova line. See Rudy et al. (2002b) and Lynch et al. (2004).

initially grew in strength, before reaching a maximum about 15 days after the outburst, and then decreased monotonically. The higher excitation neutral species of He I started out weak even at maximum light and only later reached their maximum, in this case about 23 days after peak brightness. [Ne II], the first of the nebular lines to appear, may be present even at early stages but clearly strengthens much later than the He II lines. Our observations ended when the nova went behind the sun, so we do not know when the [Ne II] line reached maximum strength.

11. MODELS OF THE NOVA

Based on the SpeX observations, a model of the ejecta was developed in Cloudy (Ferland et al. 1998). We assumed that V1187 Sco was a classical nova with a spherical Hubble-type expansion distribution and reasonable values for the elemental enhancements. The emission was reasonably well fitted using a mass of order $10^{-4}\,M_{\odot}$. A full photoionization analysis will be presented in a later paper from data obtained when the nova reaches its full nebular phase.

The line profiles showed an unusual evolution compared to that seen for ultraviolet resonance lines of recent novae studied with the Goddard High Resolution Spectrograph and the Space Telescope Imaging Spectrograph, V1974 Cyg 1992 (Shore et al. 1993) and V382 Vel (Shore et al. 2003), for which the velocity resolution and coverage of the early outburst were comparable to V1187 Sco. The UV lines showed that the ejecta display a linear velocity law with radius, $v = kr$, where r is the radial distance and a density variation that scales as $\rho = kr^{-3}$ after the initial fireball stage (e.g., Hauschildt et al. 1997). The lines initially narrowed as the highest velocity material contributed progressively less to the profile. In general, the same spectral structure—presumably from discrete emission elements—was visible on all line profiles after the transition to the nebular stage.

The line profiles in V1187 Sco were simulated using a Monte Carlo code (Shore et al. 1993, 2003) for spherical shells and planar disks (Fig. 18). The free parameters were the maximum velocity, the maximum density, the fractional thickness $\Delta r/r$ of the ejecta, and the emission law for the line (whether the intensity depends linearly or quadratically on the density). The maximum density was scaled to unity, and the maximum velocity was a free parameter. Figure 19 shows line profiles computed with a maximum velocity of 3000 km s^{-1} to match the early FWHM of the optical lines. The profiles assume two simple geometries, spherical (*left*) and a planar disk viewed edge-on (*right*) and use about 30,000 emission elements distributed in three dimensions within the shell/disk according to the density law. The last profile in each column is an observed Paβ line profile, for August 13 (*left*) and September 30 (*right*) (the first and last SpeX data; see Table 1). For each geometry we used three different radial widths for the ejecta, $\Delta r/r = 0.2$ (*top*), 0.5 (*second from top*), and 0.7 (*third from top*).

If the initial geometry was spherical, the maximum velocity of the ejecta may have been higher than that reported in the early optical observations. To show this, we present in Figure 20 another simulated profile. As a comparison with the first Paβ profile, we show an alternative profile for which the ejecta were assumed to have $\Delta r/r = 0.7$ and a maximum velocity of 6000 km s^{-1}. The highest velocity gas is not seen; the bulk of the emission comes from the inner part of the relatively geometrically thick ejecta. There are no spectra showing P Cygni absorption profiles, which

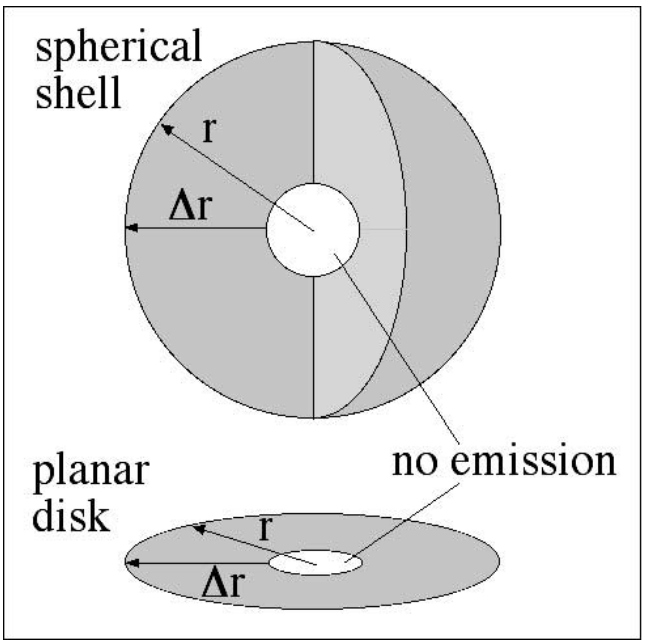

FIG. 18.—Geometries modeled and shown in Figs. 19 and 20.

we have previously used to constrain the maximum velocity of the ejecta, so we cannot present a unique solution for the shell from the line profiles alone but indicate a possible variation of the geometry of the shell during the ejection.

For comparison, the line profiles of V1974 Cyg were generally symmetric and showed a progression in time similar to that seen here, from initially flat or round-topped profiles to spikes profiles. A possible explanation is a change in the overall geometry of the emitting gas. If as appears to be the case in other novae, the highest velocity gas is more spherical than the slower, inner material, the profiles would show the progression we observe in V1187 Sco. Once spatially resolved, nova ejecta are often axisymmetric lobes, as in HR Del 1967, or rings, as in DQ Her 1934 and V1974 Cyg 1992.

12. SUMMARY AND CONCLUSIONS

V1187 Sco was a rapidly evolving ONeMg nova ($t_2 < 8$ days) that did not form dust before entering its coronal (nebular) phase. The unprecedented time and wavelength coverage (27 spectra in the 0.38–36 μm range in the first 58 days after peak brightness) reveal daily and weekly changes in the relative strengths of the emission lines that should provide a framework for detailed theoretical modeling of the ejecta. Included in the observations are the first-ever spectrum of a nova in outburst from the *Spitzer Space Telescope* and the earliest time series of novae spectra in the 8–13 μm region. The time series provides quantitative measurements of a variety of line strengths as a function of time, results that should constrain the physical parameters of the ejecta (electron temperature, density, illuminating radiation field, etc.) and their changes with time. A key finding in this study was the time evolution of the He I lines at 1.0830 and 2.0581 μm. Unlike the other lines in the spectra, these lines followed a complicated route covering several weeks in which the lines strengthened and broadened. Modeling of the doubled emission lines of H I suggests that the ejecta was in the form of a physically thick (radially) body like a ring or partial sphere. A summary of the findings is given in Table 6.

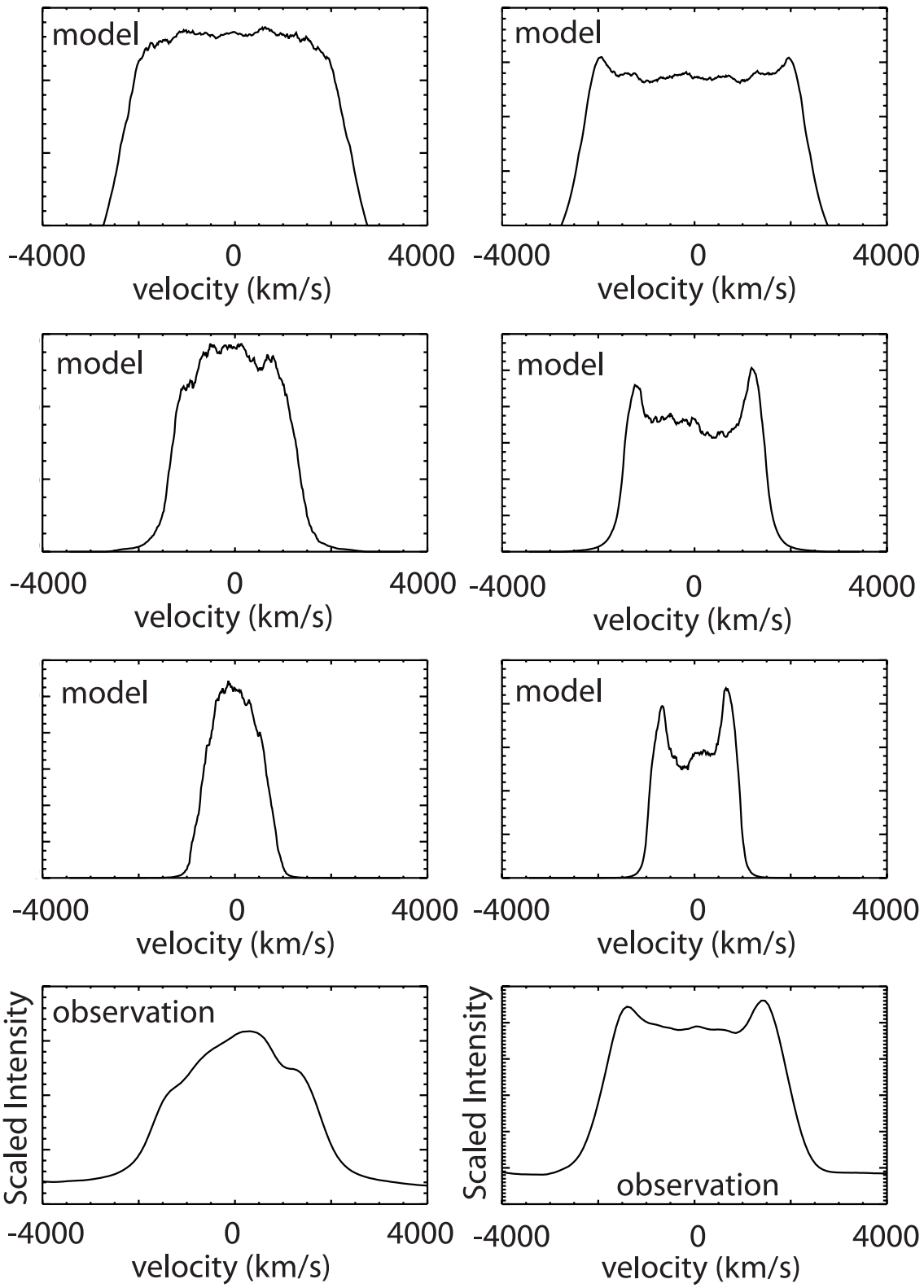

FIG. 19.—Comparison of model line profiles with Paβ from two epochs (*bottom*: *left*, 2004 August 13; *right*, 2004 September 30). The models are shown in the top three rows for three different fractional thicknesses. The order, from top, is $\Delta r/r = 0.2$, 0.5, and 0.7. All profiles have the same maximum expansion velocity, 3000 km s^{-1}. The left column shows the results for spherical shells; the right shows the results for annuli. See text for more discussion.

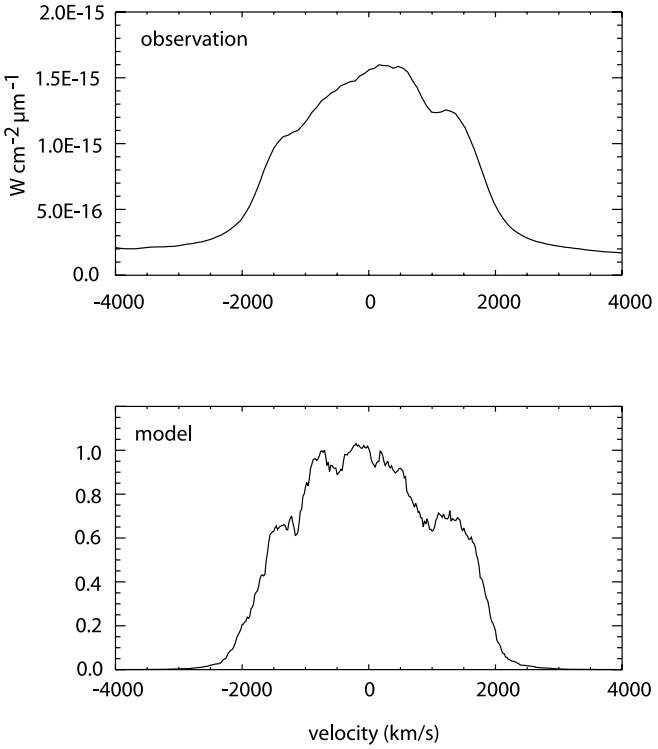

FIG. 20.—Comparison of Paβ for August 13 (*top*) with a high maximum expansion velocity, 6000 km s^{-1}, spherical shell with $\Delta r/r = 0.7$. This highlights the uncertainties in determining maximum expansion velocities from FWHM measurements in the optically thin stages of the outburst; the highest velocity gas is not seen since the bulk of the emission comes from the inner part of the ejecta.

TABLE 6
NOVA SUMMARY

Parameter	Value
Name	V1187 Scorpii, Nova Scorpii 2004 No. 2
Discovered	2004 Aug 3.583 UT (JD 2,453,221.08)
Date of peak (estimated)	2004 Aug 3.583 UT (JD 2,453,221.08)
Equatorial coordinates	17 29 18.81, −31 46 01.5 (J2000.0)
Galactic coordinates	355.7241, 1.4505 (G2000.0)
Speed class	Very fast
t_2	<8.7 days
t_3	<15.0 days
White dwarf	ONeMg, $M > 1.0\ M_\odot$
Secondary star	Unknown
Emission lines	Complex, doubled profiles
Line widths (FWHM)	4500 km s^{-1}
Ejecta mass	$\sim 10^{-4}\ M_\odot$
Reddening $E(B-V)$	1.56 ± 0.08
Extinction A_V	4.68 ± 0.24, assuming $A_V/E(B-V) = 3.05$
Distance	5.3 ± 0.6 kpc
Dust formation	No

NOTE.—Units of right ascension are hours, minutes, and seconds, and units of declination are degrees, arcminutes, and arcseconds.

The authors would like to thank Alan Tokunaga for granting us many unscheduled nights of observing time to monitor the nova. Also due thanks are the IRTF telescope operators Dave Griep, Bill Golisch, and Paul Sears for extending their hours for us. Daryl Kim, Eric Nelson, and Laurie Nelson provided valuable logistic support. Bo Reipurth kindly relinquished part of one night for us to make SpeX observations. David Dearborn helped with many discussion of TNRs. D. K. L., R. W. R., M. L. S., R. B. P., R. D. G., N. S., and T. E. H. were Visiting Astronomers at the Infrared Telescope Facility, operated by the University of Hawaii under Cooperative Agreement NCC 5-538 with the NASA, Office of Space Science, Planetary Astronomy Program. We are grateful to Jean Rene Roy, who made Gemini North's Michelle spectrograph available to us on very short notice. This paper is based in part on observations obtained at the Gemini Observatory, which is operated by the Association of Universities for Research in Astronomy, Inc., under a cooperative agreement with the National Science Foundation (NSF) on behalf of the Gemini partnership: the NSF (United States), the Particle Physics and Astronomy Research Council (PPARC) (United Kingdom), the National Research Council (Canada), CONICYT (Chile), the Australian Research Council (Australia), CNPq (Brazil), and CONICET (Argentina). The UKIRT is operated by the Joint Astronomy Centre on behalf of the UK PPARC. The W. M. Keck Observatory is operated as a scientific partnership among the California Institute of Technology, the University of California, and NASA. The Observatory was made possible by the generous financial support of the W. M. Keck Foundation. This work is based, in part, on observations made with the *Spitzer Space Telescope*, which is operated by the Jet Propulsion Laboratory (JPL), California Institute of Technology under NASA contract 1407. Support for this work was provided by NASA through contract number 1267992 issued by the JPL/California Institute of Technology. This publication makes use of data products from 2MASS, which is a joint project of the University of Massachusetts and the Infrared Processing and Analysis Center/California Institute of Technology, funded by NASA and the NSF. The Image Reduction and Analysis Facility (IRAF) is written and supported by the IRAF programming group at the National Optical Astronomy Observatory (NOAO) in Tucson, Arizona. NOAO is operated by the Association of Universities for Research in Astronomy, Inc., under cooperative agreement with the NSF. We acknowledge with thanks the variable star observations from the AAVSO International Database contributed by observers worldwide and used in this research. S. S. is grateful for partial support from NSF and NASA grants to Arizona State University. The Liverpool Telescope is funded through EU, PPARC, and Liverpool John Moores University grants and the generous benefaction of A. E. Robarts. M. F. B. and R. Z. acknowledge support through a PPARC Senior Fellowship and a PPARC Postdoctoral Research Assistantship, respectively. We thank Iain Steele for assistance with securing the Liverpool Telescope observations. This work was supported under the Aerospace Corporation's Independent Research and Development Program and under the Aerospace Corporation's Mission Oriented Investigation and Experimentation program, funded by the US Air Force Space and Missile Systems Center under Contract FA8802-04-C-0001.

Facilities: IRTF (BASS, Spex), Gemini:Gillett (Michelle), Keck:II (NIRSPEC), UKIRT (CGS4), *Spitzer* (IRS), MMT (Blue channel spectrograph)

REFERENCES

Austin, S. J., Wagner, R. M., Starrfield, S., Shore, S. N., Sonneborn, G., & Bertram, R. 1996, AJ, 111, 869
Bowen, I. S. 1947, PASP, 59, 196
Capaccioli, M., della Valle, M., Rosino, L., & D'Onofrio, M. 1989, AJ, 97, 1622
Cohen, J. G. 1985, ApJ, 292, 90
Cohen, M., Walker, R. G., Barlow, M. J., & Deacon, J. R. 1992a, AJ, 104, 1650
Cohen, M., Walker, R. G., & Witteborn, F. C. 1992b, AJ, 104, 2030
Cohen, M., Witteborn, F. C., Carbon, D. F., Davies, J. K., Wooden, D., & Bregman, J. 1996, AJ, 112, 2274
Cohen, M., Witteborn, F. C., Roush, T., Bregman, J., & Wooden, D. 1998, AJ, 115, 1671
Cohen, M., Witteborn, F. C., Walker, R. G., Bregman, J., & Wooden, D. 1995, AJ, 110, 275
Cushing, M. C., Vacca, W. D., & Rayner, J. T. 2004, PASP, 116, 362
Draine, B. T. 1989, in Proc. 22nd ESLAB Symp. on Infrared Spectroscopy in Astronomy, ed. B. H. Kaldeich (ESA SP-290; Noordwijk: ESA), 93
Ferland, G. J., Korista, K. T., Verner, D. A., Ferguson, J. W., Kingdon, J. B., & Verner, E. M. 1998, PASP, 110, 761
Gehrz, R. D., Truran, J. W., Williams, R. E., & Starrfield, S. 1998, PASP, 110, 3
Glasse, A. C., Atad-Ettedgui, E. I., & Harris, J. W. 1997, Proc. SPIE, 2871, 1197
González-Pérez, J. N., Kidger, M. R., & Martín-Luis, F. 2001, AJ, 122, 2055
Grandi, S. A. 1980, ApJ, 238, 10
Hackwell, J. A., et al. 1990, Proc. SPIE, 1235, 171
Harrison, T. E., & Stringfellow, G. S. 1994, ApJ, 437, 827
Hauschildt, P. H., Shore, S. N., Schwarz, G. J., Baron, E., Starrfield, S., & Allard, F. 1997, ApJ, 490, 803
Hoffleit, D., & Jaschek, D. 1982, The Bright Star Catalogue (4th ed.; New Haven: Yale Univ. Obs.)
Houck, J. R., et al. 2004, ApJS, 154, 18
Joyce, R. R. 1992, in ASP Conf. Ser. 23, Astronomical CCD Observing and Reduction Techniques, ed. S. B. Howell (San Francisco: ASP), 258
Kato, M. 2002, in ASP Conf. Ser. 261, The Physics of Cataclysmic Variables and Related Objects, ed. B. Gaensicke, K. Beuermann, & K. Reinsch (San Francisco: ASP), 595
Koornneef, J. 1983, A&A, 128, 84
Kurucz, R. L. 1991, in Precision Photometry: Astrophysics of the Galaxy, ed. A. G. D. Phillip, A. R. Upgren, & K. A. Janes (Schenectady: Davis), 27
———. 1994, CD-ROM 19, Solar Abundance Model Atmospheres for 0, 1, 2, 4, 8 km/s (Cambridge: SAO)
Lynch, D. K., Campbell, E., Mazuk, S., & Venturini, C. C. 2002, in AIP Conf. Proc. 637, Classical Nova Explosions, ed. M. Hernanz & J. José (Melville: AIP), 155
Lynch, D. K., Rudy, R. J., Venturini, C. C., Mazuk, S., & Puetter, R. C. 2001, AJ, 122, 2013
Lynch, D. K., Wilson, J. C., Rudy, R. J., Venturini, C. C., Mazuk, S., Miller, N. A., & Puetter, R. C. 2004, AJ, 127, 1089
Mazuk, S., Venturini, C. C., Rudy, R. J., Lynch, D. K., Puetter, R. C., & Perry, R. B. 2002, IAU Circ., 7945, 2
McLean, I. S., et al. 1998, Proc. SPIE, 3354, 566
Mountain, C. M., Robertson, D., Lee, T. J., & Wade, R. 1990, Proc. SPIE, 1235, 25
Munari, U., & Zwitter, T. 1997, A&A, 318, 269
Payne-Gaposchkin, C. 1957, The Galactic Novae (Amsterdam: North-Holland)
Rayner, J. T., Toomey, D. W., Onaka, P. M., Denault, A. J., Stahlberger, W. E., Vacca, W. D., Cushing, M. C., & Wang, S. 2003, PASP, 115, 362
Rossano, G. S., Rudy, R. J., Puetter, R. C., & Lynch, D. K. 1994, AJ, 107, 1128
Rudy, R. J., Dimpfl, W. L., Lynch, D. K., Mazuk, S., Venturini, C. C., Wilson, J. C., Puetter, R. C., & Perry, R. B. 2003, ApJ, 596, 1229
Rudy, R. J., Erwin, P., Rossano, G. S., & Puetter, R. C. 1991, ApJ, 383, 344
Rudy, R. J., Lynch, D. K., Mazuk, S., Venturini, C. C., Puetter, R. C., & Perry, R. B. 2002a, AAS Meeting 201, 40.06
Rudy, R. J., Venturini, C. C., Lynch, D. K., Mazuk, S., & Puetter, R. C. 2002b, ApJ, 573, 794
Savage, B. D., & Mathis, J. S. 1979, ARA&A, 17, 73
Schmidt, G. D., Weymann, R. J., & Foltz, C. B. 1989, PASP, 101, 713
Schmidt, T. 1957, Z. Astrophys., 41, 182
Schwarz, G. J. 2002, ApJ, 577, 940
Schwarz, G. J., Shore, S. N., Starrfield, S., Hauschildt, P. H., Della Valle, M., & Baron, E. 2001, MNRAS, 320, 103
Shore, S. N., Sonneborn, G., Starrfield, S., Gonazlez-Riestra, R., & Ake, T. B. 1993, AJ, 106, 2408
Shore, S. N., et al. 2003, AJ, 125, 1507
Szkody, P. 1994, AJ, 108, 639
Tokunaga, A. 2000, in Allen's Astrophysical Quantities, ed. A. N. Cox (4th ed.; New York: Springer), 143
van den Bergh, S., & Younger, P. F. 1987, A&AS, 70, 125
Vanlandingham, K. M., Schwarz, G. J., Shore, S. N., Starrfield, S., & Wagner, R. M. 2005, ApJ, 624, 914
Vanlandingham, K. M., Starrfield, S., & Shore, S. N. 1997, MNRAS, 290, 87
Vanlandingham, K. M., Starrfield, S., Shore, S. N., & Sonneborn, G. 1999, MNRAS, 308, 577
Vanlandingham, K. M., Starrfield, S., Wagner, R. M., Shore, S. N., & Sonneborn, G. 1996, MNRAS, 282, 563
Venturini, C. C., Rudy, R. J., Lynch, D. K., Mazuk, S. M., & Puetter, R. C. 2004, AJ, 128, 405
Warner, B. 1989, in Classical Novae, ed. M. F. Bode & A. Evans (Chichister: Wiley), 1
Werner, M. W., et al. 2004, ApJS, 154, 1
Williams, P. M., Longmore, A. J., & Geballe, T. R. 1996, MNRAS, 279, 804
Woodward, C. E., et al. 1995, ApJ, 438, 921
Yamaoka, H. 2004, IAU Circ., 8380, 1
Yamaoka, H., Itagaki, K., Fujii, M., & Liller, W. 2004, IAU Circ., 8381, 3
Zamanov, R. K., Bode, M., Steele, I. A., & O'Brien, T. J. 2004, IAU Circ., 8415, 3